RESEARCH ARTICLE doi.org/10.1002/adsc.202200870

Advanced Synthesis & Catalysis

Very Important Publication

Filling the Gaps in the Challenging Asymmetric Hydrogenation of Exocyclic Benzofused Alkenes with Ir–P,N Catalysts

Maria Biosca,[+a] Pol de la Cruz-Sánchez,[+a] Daniel Tarr,[a] Patricia Llanes,[b] Erik A. Karlsson,[b] Jèssica Margalef,[a] Oscar Pàmies,[a] Miquel A. Pericàs,[a,*] and Montserrat Diéguez[a,*]

[a] Departament de Química Física i Inorgànica, Universitat Rovira i Virgili, C/Marcel·lí Domingo 1, 43007 Tarragona, Spain
Phone: (+34)977558780; Fax: (+34)955559563
E-mail: miquelangel.pericas@urv.cat; montserrat.dieguez@urv.cat

[b] Institute of Chemical Research of Catalonia (ICIQ), The Barcelona Institute of Science and Technology, Av Països Catalans 16, 43007 Tarragona, Spain

[+] These authors contributed equally to this study.

Manuscript received: August 7, 2022; Revised manuscript received: September 22, 2022;
Version of record online: October 11, 2022

Supporting information for this article is available on the WWW under https://doi.org/10.1002/adsc.202200870

Abstract: Herein, we report a chiral phosphine-triazole ligand for the Ir-catalyzed asymmetric hydrogenation of exocyclic benzofused alkenes. Overcoming previous limitations, the catalytic system is able to successfully hydrogenate exocyclic olefins bearing a benzofused five- and six-membered ring motif (ee's between 92 to 99%). The catalyst tolerates well the presence of several substituents and substitution patterns at both aromatic rings. The absence of a competing isomerization process together with the perfect fit of the olefins in the catalyst chiral pocket are key to surpass the previous limitations in the hydrogenation of both 5- and 6-membered ring benzofused exocyclic olefins.

Keywords: Exocyclic olefins; asymmetric hydrogenation; iridium; P,N-ligands; deuterogenation; DFT calculations

Introduction

The metal-catalyzed asymmetric hydrogenation (AH) of alkenes is still a growing field. It offers some of the most sustainable and straightforward processes for producing a broad range of pharmaceuticals and fine chemicals, which justify the interest of top pharmaceutical companies.[1] A thorough patent review by Glorius, Leker et al. recently highlighted the industrial relevance of asymmetric hydrogenation.[2] They concluded that catalytic hydrogenation is a mature technology that yet has to reach its maximum economic relevance and will continue to generate valuable patents and innovations.

In this respect, to fully exploit the application of asymmetric hydrogenation there is still a constant need to expand the range of substrates undergoing the process with high enantioselectivity, thus making the synthesis of the most diverse chiral molecules possible. Whereas the asymmetric hydrogenation of functionalized olefins has a long story, and their catalysts can efficiently reduce olefins with very diverse structures,[3] the reduction of non-chelating olefins (the so called unfunctionalized olefins) is less mature and has therefore led to fewer synthetic applications.[4] The development of Ir-catalysts modified with chiral heterodonor ligands (mainly P,N-ligands) opened the possibility to hydrogenate non-chelating olefins, which was not feasible with classical Rh- and Ru-diphosphine

catalysts.[4] Since then, many efforts have been devoted to extend the substrate scope by developing new catalyst types.

Among the most challenging unfunctionalized substrates, the exocyclic olefins containing a benzofused five/six-membered ring motif, whose hydrogenation products are present in pharmaceutical natural products and key bioactive drug intermediates (Figure 1), represent an unmet goal.[5] Compared to the considerable number of reports dealing with the reduction of unfunctionalized acyclic and endocyclic olefins, the reduction of unfunctionalized exocyclic olefins is clearly underdeveloped. Only a few publications have reported high catalytic performance, albeit with a limited substrate scope, the Ir/In-BiphPHOX catalyst being the one with comparatively broader scope (Figure 2).[6] Thus, the latter catalyst is able to hydrogenate a range of olefins exocyclic to a five-membered benzofused ring with high enantioselectivities (93–98% ee).[6a] However, the recorded enantioselectivities sharply decreased when an *ortho* substituent was present on the aromatic ring (Ar group in Figure 2, top) and was also lower in the reduction of the parent olefin exocyclic to a benzofused six-membered olefin (75% ee). Note that a similar ring size dependence has been observed in the hydrogenation of other olefins with an exocyclic double bond such as α,β'-disubstituted unsaturated lactones and lactams.[4g,7] Additionally, the reaction required an additive and a specific solvent (*o*-xylene), moving away from the commonly used solvents in Ir-catalyzed asymmetric hydrogenation. The difficulty in the reduction of this type of exocyclic olefins at benzofused five/six-membered rings is even more evident if we consider that PHOX, which are the most successful ligands for Ir-catalyzed hydrogenation, did not work in these cases.[6a]

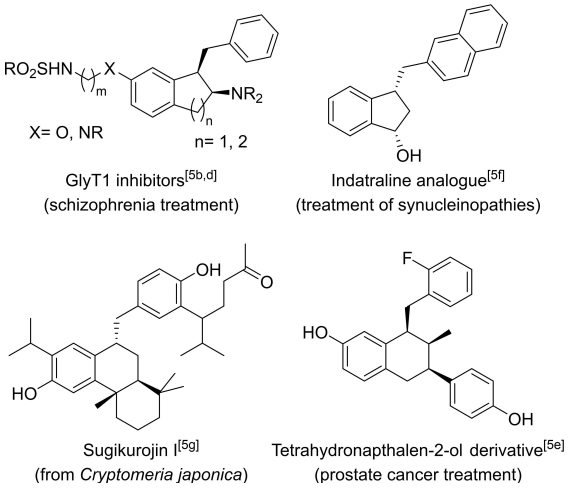

Figure 1. Representative examples of natural occurring compounds and drugs containing a chiral benzofused five/six-membered ring motif.

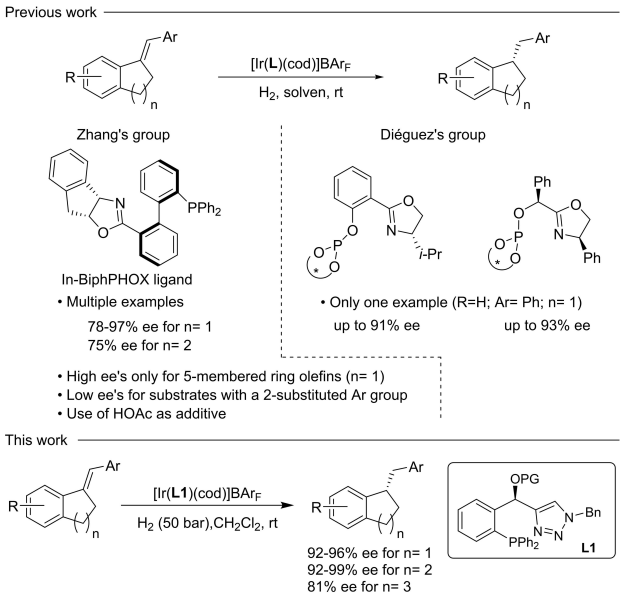

Figure 2. Precedents in the Ir-catalyzed asymmetric hydrogenation of unfunctionalized exocyclic olefins.

In 2008, we started a research line to address the asymmetric hydrogenation of non-chelating olefins, with the ultimate goal of achieving high enantioselectivity in the reduction of previously unsolved substrates. Under the concept of tailor-made ligands which can be systematically modified to introduce specific structural patterns that adapt to the particularities of each substrate type, we have been able to improve the catalytic performance for a range of challenging olefins, going from the most elusive 1,1'-disubstituted to the tetrasubstituted ones.[6c,8] Herein, we report a new P,N-ligand design specially well suited for the Ir-catalyzed hydrogenation of exocyclic olefins at benzofused five-membered rings, the more challenging analogues involving six-membered rings, and with promising results for a seven-membered analogue (Figure 2, bottom). The new phosphine-triazole ligands **L1** are based on the phosphine-oxazolines PHOX in which a chiral carbon spacer has been added between the oxazoline and the phenyl ring to study how the size of the chelate ring influences the catalytic performance. The ligand design has been completed by attaching a silyl group on the carbon spacer. This latter design feature was inspired by Pfaltz's first generation of phosphine-pyridine design that showed that the silyl groups are interacting with the active site of the catalysts and therefore they have shown to be important in their success.[9] In addition, the oxazoline moiety in the PHOX ligand has also been replaced by a triazole with the aim to facilitate the stabilization of the substrate in the catalyst chiral pocket via N–H interactions.[10] We have also performed mechanistic studies (deuterogenation experiments and DFT calcu-

lations) to explain the origin of enantioselectivity in the reactions mediated by ligands **L1**.

Results and Discussion

Synthesis of Ligands and Ir(I)-Catalyst Precursors

The synthesis of the new phosphine-triazole ligands **L1a–b** is straightforward from (*R*)-(1-benzyl-1*H*-1,2,3-triazol-4-yl)(2-iodophenyl)methanol **1** (Scheme 1). Compound **1** was synthesized from the readily accessible 2-iodobenzaldehyde using a simple three step procedure developed by Pericàs and Nachtsheim groups.[11] Thus, the synthesis of enantiopure **1** (> 99.9% ee) involves the non-enantioselective propargylation of 2-iodobenzaldehyde, the CALB-catalyzed enzymatic kinetic resolution of the intermediate propargyl alcohol, and a final Cu-catalyzed alkyne-azide Huisgen-type cycloaddition. Then, the Pd-catalyzed phosphination of **1** gave the corresponding phosphine-triazole compound **2** in 78% yield. Finally, the hydroxyl group in **2** was protected with two different bulky silyl ether groups (TIPS and TBS) to yield the desired enantiopure phosphine-triazole ligands **L1a** and **L1b** in 78% and 91% yield, respectively.

Coordination of ligands **L1a–b** to iridium using $[Ir(\mu\text{-}Cl)(cod)]_2$ as precursor in dichloromethane at room temperature, followed by the replacement of the Cl anion by BAr_F^- using $NaBAr_F$ in an aqueous suspension led to desired Ir-catalyst precursors (Scheme 1). Advantageously, they were obtained as orange air stable solids. They were therefore handled and stored in air. The formation of ligands and Ir-complexes was confirmed by ^1H, ^{13}C and ^{31}P NMR spectroscopy and HRMS-ESI spectrometry (see experimental and SI section for details). The HRMS-ESI spectra agree with the assigned structures displaying the heaviest ions at m/z values corresponding to the loss of BAr_F anion.

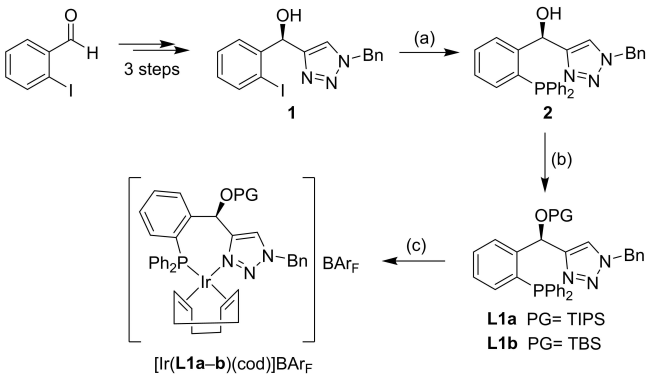

Scheme 1. Synthesis of ligands **L1a–b** and of [Ir(**L1**)(cod)]BAr_F catalyst precursors. a) $Pd_2(dba)_3$, dippf, $HPPh_2$, NEt_3, toluene, 110 °C, 2.5 h. b) TIPSOTf or TBSOTf, 2,6-lutidine, CH_2Cl_2, rt, 2 h. c) $[Ir(\mu\text{-}Cl)(cod)]_2$, CH_2Cl_2, reflux, 1 h then $NaBAr_F$, H_2O, rt, 30 min.

Initial Catalytic Screening. Ir-Catalyzed Asymmetric Hydrogenation of Two Model Exocyclic Olefins S1 and S2

The Ir-catalyst precursors containing phosphine-triazole ligands **L1a–b** were first tested in the hydrogenation of olefins **S1** (exocyclic to a benzofused five-membered ring) and the more challenging **S2** (exocyclic to a 1,2,3,4-tetrahydronaphthalene analogue). The results are summarized in Table 1, entries 1–4. We applied in these experiments the most commonly used reaction conditions in the Ir-catalyzed asymmetric hydrogenation of unfunctionalized olefins (50 bar of H_2 at room temperature using dichloromethane and 1 mol% of the catalysts precursor [Ir(cod)(**L1**)]BAr_F).[6b] Positively, full conversion and high enantioselectivities (ee's up to 99%) in both substrate types were achieved by selecting the right silyl group, in only 4 hours and without any additive.

We next studied the effect of the hydrogen pressure on the catalytic outcome (entries 5–8). The results show a small decrease in conversion and enantioselectivity when the hydrogen pressure was lowered to 10 bars (Table 1, entries 5 and 6). Nevertheless, the catalytic performance is not affected by increasing the hydrogen pressure (entries 7 and 8).

For comparison purposes, we also studied whether the high enantioselectivities achieved in the hydrogenation of **S1** using previously reported ligands **L2**[6b] and **L3**[6c] were maintained in the hydrogenation of 6-membered ring analogue **S2** (Table 1; entries 10 and 12). In line with previous results using Ir/In-BiphPHOX catalysts,[6a] the use of both Ir-phosphite-oxazoline based catalysts provided lower enantiocontrol in the hydrogenation of **S2** than for **S1** (entries 9 and 11 vs 10 and 12, respectively).

Scope and Limitations. Ir-Catalyzed Asymmetric Hydrogenation of a Range of Benzofused-Based Exocyclic Olefins

We next studied the scope of the Ir/**L1b** catalytic system by extending our work to the hydrogenation of other exocyclic olefins based on benzofused systems with different ring sizes and diverse substituents at both aromatic rings present in the structures of the substrates.

We initially considered the reduction of various double bonds exocyclic to a benzofused five-membered ring (**S3**–**S9**; Table 2, entries 1–7). As observed for the Ir/In-BiphPHOX system,[6a] Ir/**L1b** tolerates very well the presence of several substituents and substitution patterns at both aromatic rings (**S3**–**S8**). In addition, note that improving the performance of the

Table 1. Asymmetric hydrogenation of olefins **S1** and **S2**.[a]

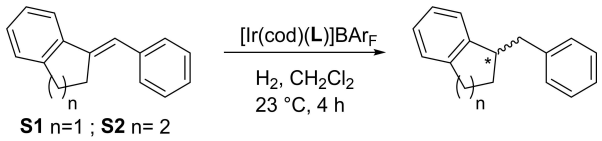

Entry	Substrate	H_2 (bar)	L	%Conv[b]	%ee[c]
1	**S1**	50	**L1a**	100	85 (*S*)
2	**S1**	50	**L1b**	100 (98)	95 (*S*)
3	**S2**	50	**L1a**	100	87 (*S*)
4	**S2**	50	**L1b**	100 (97)	99 (*S*)
5	**S1**	10	**L1b**	99	92 (*S*)
6	**S2**	10	**L1b**	88	95 (*S*)
7	**S1**	75	**L1b**	100	95 (*S*)
8	**S2**	75	**L1b**	100	99 (*S*)
9[d]	**S1**	50	**L2**	100	91 (*R*)
10	**S2**	50	**L2**	95	87 (*R*)
11[e]	**S1**	50	**L3**	100	93 (*S*)
12	**S2**	50	**L3**	79	30 (*S*)

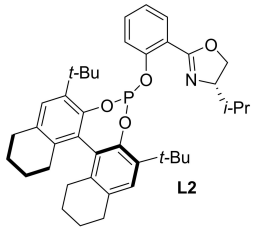

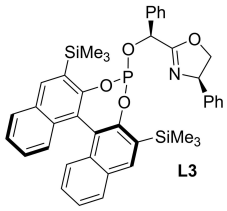

[a] Reaction conditions: 1 mol% [Ir(cod)(**L**)]BAr$_F$, CH_2Cl_2 as solvent at 23 °C for 4 h.
[b] Conversions measured by ^{1}H NMR. Isolated yields in parenthesis.
[c] Enantiomeric excesses determined by chiral HPLC.
[d] Data from ref. [6b].
[e] Data from ref. [6c].

Table 2. Asymmetric hydrogenation of benzylidene-containing 2,3-dihydro-1*H*-indenes **S3**–**S8** and 2,3-dihydrobenzofuran **S9**.[a]

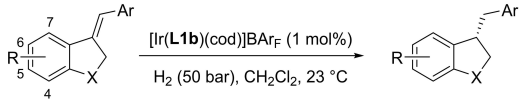

Entry	Subs.	Ar	R	X	%Yield	%ee[b]
1	**S3**	4-Me–C_6H_4	H	CH_2	98	93 (*S*)
2	**S4**	4-Cl–C_6H_4	H	CH_2	99	94 (*S*)
3	**S5**	4-OMe–C_6H_4	H	CH_2	97	94 (*S*)
4	**S6**	3-Me–C_6H_4	H	CH_2	97	96 (*S*)
5	**S7**	2-Me–C_6H_4	H	CH_2	99	95 (*S*)
6	**S8**	C_6H_5	5-Br	CH_2	98	92 (*S*)
7	**S9**	C_6H_5	H	O	95	95 (*S*)

[a] Full conversions were attained in all cases after 4 h.
[b] Enantiomeric excesses determined by chiral HPLC.

Ir/In-BiphPHOX, whose ability to hydrogenate substrates with *ortho* substituents on the aromatic ring (Ar group) is not optimal (ee's up to 78%), the Ir/**L1b** was also able to provide high enantioselectivity in the reduction of substrate **S7**, bearing such an *ortho* substituent (95% ee, entry 5). Finally, the enantiomeric outcome was also maintained in the reduction of the dihydrobenzofuran analogue **S9** (95% ee, entry 7).

We next applied Ir/**L1b** in the hydrogenation of a series of olefins with the double bond exocyclic to a benzofused six-membered ring (Table 3). Positively, the catalytic performance was highly independent of

Table 3. Asymmetric hydrogenation of benzylidene-1,2,3,4-tetrahydronaphtalenes **S10**–**S18**.[a]

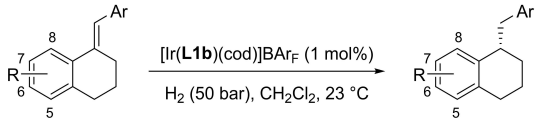

Entry	Subs.	Ar	R	%Yield	%ee[b]
1	**S10**	4-Me–C_6H_4	H	97	98 (*S*)
2	**S11**	4-Cl–C_6H_4	H	99	99 (*S*)
3	**S12**	3-Me–C_6H_4	H	96	98 (*S*)
4	**S13**	2-Me–C_6H_4	H	97	92 (*S*)
5	**S14**	C_6H_5	5-Br	97	98 (*S*)
6	**S15**	C_6H_5	5-OMe	98	99 (*S*)
7	**S16**	C_6H_5	6-Br	96	99 (*S*)
8	**S17**	C_6H_5	7-Br	99	98 (*S*)
9	**S18**	C_6H_5	7-OMe	98	98 (*S*)

[a] Full conversions were attained in all cases after 4 h.
[b] Enantiomeric excesses determined by chiral HPLC.

the substitution pattern of the Ar group (**S10**–**S13**, ee's up to 99%). Although the hydrogenation of the *ortho*-substituted derivative **S13** led to the lowest enantioselectivity (ee's up to 92%,) this is still remarkable for this challenging substrate. An electronegative, yet π-donating chloro substituent (entry 2) was also well tolerated (99% ee). We were also pleased to find that Ir/**L1b** tolerates well variations in the substitution pattern at the fused benzene ring (**S14**–**S18**, ≥98% ee).

To explore the possibilities beyond those already described for the Ir/**L1b** catalytic system, we studied the hydrogenation of exocyclic olefins with an even larger benzofused seven-membered ring (**S19**) and, with a benzofused four-membered ring (**S20**, Scheme 2). Whereas the hydrogenation of **S20** provided the hydrogenated product with moderate enantioselectivity (40% ee), the hydrogenation of **S19** proceed with a remarkable enantioselectivity of 81% ee.

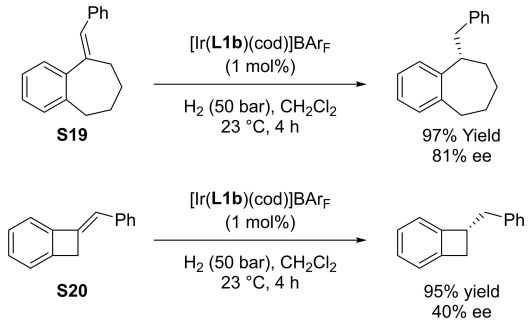

Scheme 2. Asymmetric hydrogenation of (*E*)-5-benzylidene-6,7,8,9-tetrahydro-5*H*-benzo[7]annulene **S19** and (*E*)-7-benzylidenebicyclo[4.2.0]octa-1,3,5-triene **S20**. Full conversions were attained in both cases.

Finally, having in mind that the enantiocontrol in the hydrogenation of non-chelating olefins is drastically affected by the olefin geometry,[4e,g] we studied the asymmetric hydrogenation of the *Z*-olefins **S21**–**S23** (Scheme 3). In line with previous reports, the hydrogenation of these *Z*-analogues led to much lower enantioselectivities than the *E*-analogues.

Mechanistic Insights

The elusiveness of olefins exocyclic to benzofused rings as asymmetric hydrogenation substrates has been mainly attributed to the fact that they can easily isomerize into the corresponding endocyclic olefins under hydrogenation conditions. To study if the enantioselectivities attained in the hydrogenation of *E*-olefins with different ring size could be related to the isomerization extent, we studied the deuterogenation of olefins **S3**, **S10**, **S19** and **S20** (Scheme 4).

The deuterium incorporation was only observed in the olefinic carbons, indicating that isomerization does

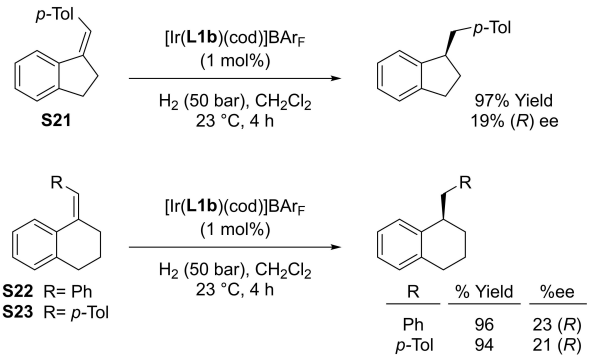

Scheme 3. Asymmetric hydrogenation of exocyclic olefins with *Z*-geometry. Full conversions were attained in all cases.

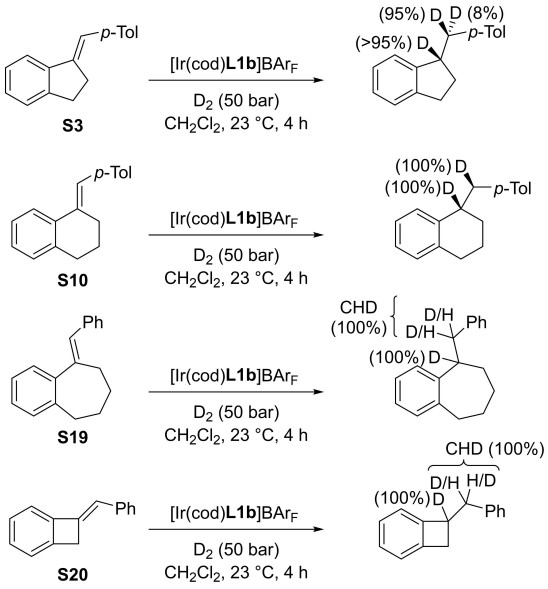

Scheme 4. Deuterogenation experiments.

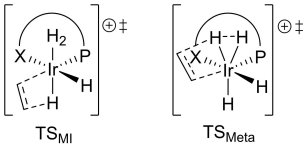

Figure 3. Schematic representation of the TSs for the migratory insertion (TS$_{MI}$) and σ-bond metathesis (TS$_{Meta}$) pathways.

not take place regardless of the size of the benzofused ring. This clearly indicates that the enantioselectivity is mainly governed by the constrains of the catalyst chiral pocket. To gain further insight about the effect of the ligand structure on this chiral pocket, we performed a DFT study of the species involved in the enantiodetermining step. Mechanistically, it has been shown that the Ir-catalyzed hydrogenation of non chelating olefins proceeds via the Ir(III)/Ir(V) catalytic cycle, where the enantioselectivity is determined in the first hydrogen transfer from the metal to the coordinated olefin.[8c,12] This step, however, can be accomplished via migratory insertion (TS$_{MI}$) or via σ-bond metathesis (TS$_{Meta}$, Figure 3).[8c,12] We therefore computed all the transition states (TSs) for both pathways with Ir/**L1b** catalyst using substrate **S2**.

The results show that the migratory insertion TSs are more favorable than the σ-bond metathesis TSs (see Supporting Information). The calculated energies of the most stable isomers of the TS$_{MI}$ are shown in Table 4. These key TSs are the result of the coordination to the two enantiotopic faces (*Re* and *Si*) of the olefin, the attack of the hydride at the two olefinic carbons and the relative disposition of the hydride (up or down). For each of them, a conformational search was carried out to make sure that the conformation with the lowest energy was found.

Positively, the calculated energy difference of the two most stable TSs (**TS$_A$** and **TS$_E$**), that lead to opposite enantiomers, is in good agreement with the experimental enantioselectivity (ee of 99% (*S*), Table 1, entry 4). The factors responsible for the enantio-

Table 4. Calculated energies (kcal/mol) for transition states of the migratory insertion pathway with substrate **S2** using Ir/**L1b**.[a]

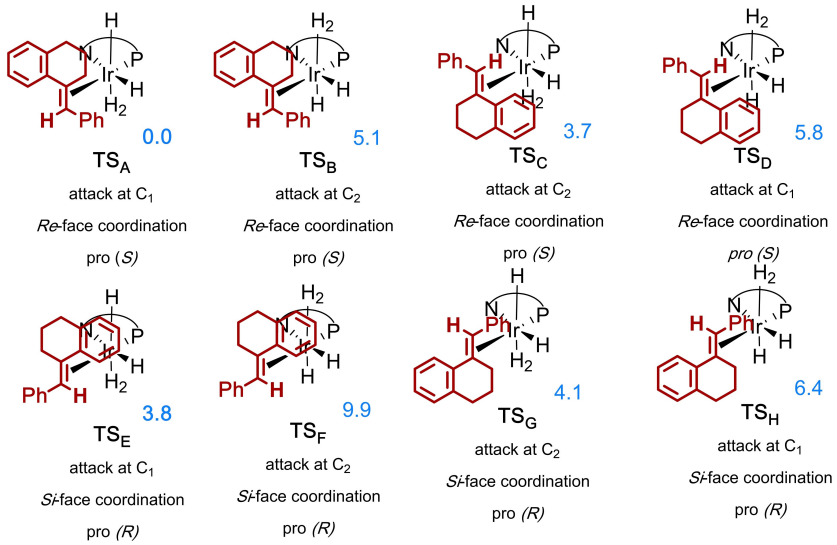

[a] C$_1$ is the olefinic carbon that is located in the ring structure and C$_2$ is the olefinic carbon that is located outside the ring structure. In all TSs the most stable conformer was selected.

selectivity can therefore be deduced by examining the structures of $\mathbf{TS_A}$ and $\mathbf{TS_E}$.

We first did a steric interaction assessment by analyzing the structures of the two most stable TSs, leading to opposite enantiomers, via a quantitative quadrant-diagram using the MolQuO software,[13] developed by Carbó et al. However, in contrast to previous studies with unfunctionalized acyclic trisubstituted olefins,[8c,14] the quadrant analysis did not provide a clear relationship between the olefin arrangement and the quadrant occupancy.

Both structures show attractive interactions between the substrate and the ligand that were analyzed with a non-covalent interaction (NCI)-plot (Figure 4). However, while the $\mathbf{TS_A}$ is stabilized by three CH–N, two CH-π and one T-shaped π–π interactions (Figure 4a), $\mathbf{TS_E}$ is only stabilized by two CH–N and one T-shaped π–π interactions (Figure 4b). Concretely, in $\mathbf{TS_A}$, two of the CH–N interactions are located between the tetrahydronaphthalene phenyl ring of the substrate and two N of the triazole moiety of the ligand, and the third CH–N interaction is found between the H of the olefinic carbon and a N of the triazole unit (see Figure 4a). These interactions show the importance of having a triazole instead of the most commonly oxazoline group into the ligand where some of these attractive CH–N interactions would not exist. Figure 4a also illustrates the T-shaped CH-π interaction of the benzyl substituent of the triazole group and two CH-π interactions of the tetrahydronaphthalene phenyl ring of the substrate with the methyl substituents of the TBS group. The presence of a TBS group in the ligand is therefore crucial.

In summary, the attractive interactions above described in $\mathbf{TS_A}$ make its chiral pocket better suited for the 6-membered exocyclic olefin **S2** than the cavity of $\mathbf{TS_E}$, where only two CH–N interactions and a T-shaped π–π interaction are found[15] (Figure 4b), whereas the attractive interactions between the substrate and the protecting silyl group are not present.

In addition, the stereochemical model also showed that the relative position of the tetrahydronaphthalene phenyl ring is important to facilitate the necessary attractive interactions in $\mathbf{TS_A}$. Ultimately, the position

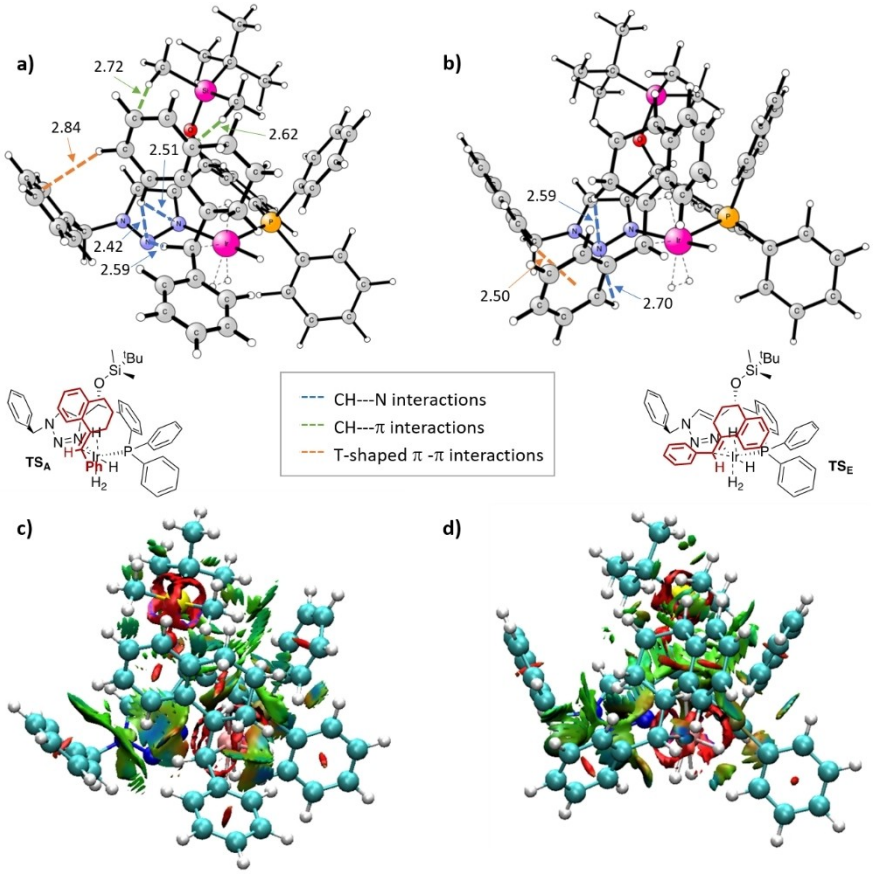

Figure 4. Optimized geometries of the most stable transition states resulting from the first hydrogen transfer from the metal to the coordinated olefin for the migratory insertion pathway for **S2** using Ir/**L1b**. (a) $\mathbf{TS_A}$: coordination from the *Re*-face, leading to the *S*-enantiomer. (b) $\mathbf{TS_E}$: coordination from the *Si*-face, leading to the *R*-enantiomer. (c) NCI plot of $\mathbf{TS_A}$. (d) NCI plot of $\mathbf{TS_E}$. For the NCI plots; strong and attractive interactions are blue, weak interactions are green and strong and repulsive interactions are red.

of this group is largely affected by the ring size of the benzofuzed moiety (Figure 5), and this can be related to the differences in the enantiomeric excesses found when the size of the benzofuzed moiety varies. While the fit in the chiral pocket is adequate for the exocyclic olefins containing a benzofused five- or six-membered ring and to a less extend the seven-membered ring, the 4-membered exocyclic substrate **S20** shifts the position of the tetrahydronaphthalene phenyl ring in such a way that results in the loss of the aforementioned attractive interactions that make $\mathbf{TS_A}$ superior.

Finally, to identify whether the low ee's achieved in the hydrogenation of *Z*-olefins compared with those of the *E*-analogues can be caused by the constrains of the catalyst chiral pocket or by the existence of isomerization, we studied the deuterogenation of *Z*-**S21** (Scheme 5). In contrast to the *E*-analogue **S3**, we observed the incorporation of deuterium at the 2-position which clearly indicates that isomerization takes place. So, we can conclude that the isomerization rate of *Z*-olefins to *E*-olefins is in the same order as hydrogenation of both isomers, which leads to low enantioselectivities.

Conclusion

In summary, we have developed an Ir/phosphine-triazole catalysts for the asymmetric hydrogenation of olefins whose double bonds are exocyclic to benzo-fused rings of different sizes. Overcoming previous limitations, we have identified a catalyst that is able to successfully hydrogenate exocyclic olefins containing a benzofused six-membered ring motif (with ee's typically of 99%). Significantly, the results also extended to olefins bearing a five-membered benzo-fused ring (ee's typically ca 95%) and for the first time a promising enantioselectivity of 81% was reached for a seven-membered benzofused analogue. Moreover, the catalyst tolerated well different substituents and substitution patterns at both aromatic rings present in the substrates, which opens up its potential use in the synthesis of high-value compounds such as drugs and natural products. The absence of a competing isomerization process together with the perfect fit of the *E*-olefins in the catalyst chiral pocket are the keys for the success of this catalyst. In this fit the presence of non-covalent attractive interactions between the substrate and the ligand components has been crucial as well as the presence in the ligand of a triazole instead of the commonly oxazoline group and a silyl group. Finally, as observed for other non-chelating functionalized olefins, the enantiomeric excess was highly dependent on the olefin geometry. Thus, the high enantioselectivities were only attained in the hydrogenation of *E*-olefins. The decrease of enantioselectivity observed for *Z*-olefins was due to an isomerization process competing with the hydrogenation.

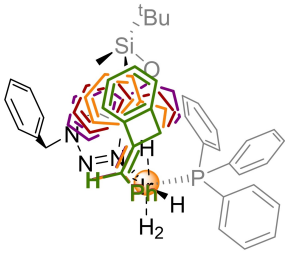

Figure 5. Representation of the effect of the substrate's size of the cycle in $\mathbf{TS_A}$. Substrates **S20** (in green), **S1** (in orange), **S2** (in red) and **S19** (in violet) are superimposed.

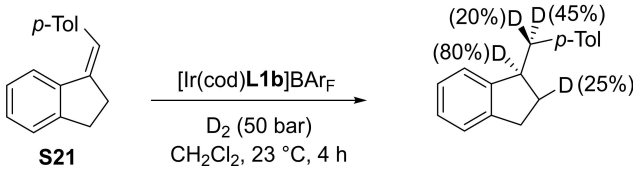

Scheme 5. Deuterogenation experiment of **S21**.

Experimental Section

General Considerations

All reactions were carried out using standard Schlenk techniques under an argon atmosphere unless otherwise noted. Solvents were purified and dried by standard procedures. Compound **1**[11] and substrates **S1**–**S4**, **S6** and **S8**–**S9**[6a] were prepared following the reported procedures. ^{1}H, ^{13}C and ^{31}P NMR spectra were recorded using a 400 MHz spectrometer. Chemical shifts are relative to that of NMR solvent for ^{1}H and $^{13}C\{^{1}H\}$ and of H_3PO_4 as internal standard for $^{31}P\{^{1}H\}$.

Synthesis of (*R*)-(1-benzyl-1*H*-1,2,3-triazol-4-yl)(2-(diphenylphosphaneyl)phenyl) Methanol 2

$Pd_2(dba)_3$ (4.58 mg, 5 μmol) and **1** (0.391 g, 1 mmol) were placed in a Schlenk tube. The tube was then entered into a N_2-filled glove box were 1,1'-bis(diisopropylphosphino)ferrocene (dippf; 4.18 mg, 10 μmol), and dry degassed toluene (2 mL) were added. After stirring for 20 min, degassed triethylamine (0.21 mL, 1.5 mmol), and diphenylphosphine (0.26 mL, 1 mmol) were added and the tube was sealed, taken out of the glove box, and heated in an oil bath at 110 °C for 2.5 h. The reaction mixture was allowed to cool to room temperature and was then kept at −20 °C overnight to induce crystallization. Filtration, followed by washing with toluene (5 × 0.5 mL), water (5 × 1 mL), and isopropanol (5 × 0.5 mL) resulted in an off-white powder that was recrystallized from hot deoxygenated isopropanol (9 mL) under Ar, filtered and washed with isopropanol (3 × 1 mL) to obtain compound **2** (0.336 g, 75% yield) as a white powder. ^{31}P NMR (162 MHz, $CDCl_3$) δ: −18.0. ^{1}H NMR (400 MHz, $CDCl_3$) δ: 3.26 (br, 1H, O*H*), 5.20 (d, 1H, $^{2}J_{H-H}$ = 14.9 Hz, CH_2Ph), 5.23 (d, 1H, $^{2}J_{H-H}$ = 14.9 Hz, CH_2Ph), 6.69 (s, 1H, C*H*=N, trz), 6.76 (d, 1H, $^{3}J_{P-H}$ = 7.2 Hz, C*H*OH), 6.95–6.98

(m, 1H, C*H*=, Ar), 7.12–7.16 (m, 4H, C*H*=, Ar), 7.19–7.24 (m, 5H, C*H*=, Ar), 7.24–7.29 (m, 1H, C*H*=, Ar), 7.29–7.34 (m, 6H, C*H*=, Ar), 7.40 (t, 1H, $^{3}J_{H-H}$ = 7.6 Hz, C*H*=, Ar), 7.68–7.71 (m, 1H, C*H*=, Ar). ^{13}C NMR (100 MHz, $CDCl_3$) δ: 53.8 (*C*H_2Ph), 66.6 (d, $^{3}J_{C-P}$ = 27.7 Hz, *C*HOH), 121.6 (*C*H=N, trz), 127.2–135.8 (aromatic carbons), 135.8 (d, $^{1}J_{C-P}$ = 11.0 Hz, *C*, Ar), 136.4 (d, $^{1}J_{C-P}$ = 11.0 Hz, *C*, Ar), 146.3 ($^{1}J_{C-P}$ = 22.0 Hz, *C*, Ar), 150.47 (*C*, Ar). MS HR-ESI [found 449.1649 $C_{28}H_{24}N_3OP$ $(M)^+$ requires 449.1652].

General Procedure for the Synthesis of Ligands L1

To a suspension of **2** (0.112 g, 0.25 mmol) in CH_2Cl_2 (1 mL), were added 2,6-lutidine (0.06 mL, 0.5 mmol) and the corresponding silyl triflate (0.3 mmol), under Ar at 0 °C. The resulting solution was then stirred 2 h at room temperature. After that time, a saturated solution of $NaHCO_3$ (2.5 ml) was added, followed by extraction with CH_2Cl_2 (3 × 2.5 mL). The combined organic phases were washed with brine (2.5 mL), dried over $MgSO_4$, concentrated, and purified with flash column chromatography (neutral SiO_2 *ca* 10 cm × 2.5 cm, 4:1 petroleum ether-EtOAc) to obtain the corresponding ligands **L1**.

(R)-1-benzyl-4-((2-(diphenylphosphaneyl)phenyl)((triisopropylsilyl)oxy)methyl)-1H-1,2,3-triazole (L1a). Reaction carried out using triisopropylsilyl trifluoromethanesulfonate (0.08 mL, 0.3 mmol). Pale-yellow oil (198 mg, 91% yield). ^{31}P NMR (162 MHz, $CDCl_3$) δ: −19.7. ^{1}H NMR (400 MHz, $CDCl_3$) δ: 0.91–0.94 (m, 18H, C*H*$_3$, *i*-Pr), 1.07 (m, 3H, C*H*, *i*-Pr), 5.13 (s, 2H, C*H*$_2$Ph), 6.72 (s, 1H, C*H*=N, trz), 6.92–7.02 (m, 6H, C*H*O, C*H*=, Ar), 7.13–7.19 (m, 6H, C*H*=, Ar), 7.28–7.30 (m, 6H, C*H*=, Ar), 7.40 (t, 1H, $^{3}J_{H-H}$ = 7.3 Hz, C*H*=, Ar), 7.99–8.03 (m, 1H, C*H*=, Ar). ^{13}C NMR (100 MHz, $CDCl_3$) δ: 12.2 (*C*H, *i*-Pr), 17.9 (*C*H$_3$, *i*-Pr), 53.5 (*C*H_2Ph), 66.5 (d, $^{3}J_{C-P}$ = 30.2 Hz, *C*H–O), 121.7 (*C*H=N, trz), 126.7–134.8 (aromatic carbons), 135.9 (d, $^{1}J_{C-P}$ = 11.0 Hz, *C*=, Ar), 137.1 (d, $^{1}J_{C-P}$ = 11.0 Hz *C*=, Ar), 148.7 ($^{1}J_{C-P}$ = 22.0 Hz, *C*=, Ar), 151.3 (*C*=, Ar). MS HR-ESI [found 605.2983 $C_{37}H_{44}N_3OPSi$ $(M)^+$ requires 605.2986].

(R)-1-benzyl-4-(((tert-butyldimethylsilyl)oxy)(2-(diphenylphosphaneyl)phenyl)methyl)-1H-1,2,3-triazole (L1b). Reaction carried out using *tert*-butyldimethylsilyl trifluoromethanesulfonate (0.07 mL, 0.3 mmol). Pale-yellow oil (118 mg, 78% yield). ^{31}P NMR (162 MHz, $CDCl_3$) δ: −19.3. ^{1}H NMR (400 MHz, $CDCl_3$) δ: −0.03 (s, 3H, C*H*$_3$, OTBS), −0.00 (s, 3H, C*H*$_3$, OTBS), 0.85 (s, 9H, *t*-Bu, OTBS), 5.13 (d, 1H, $^{2}J_{H-H}$ = 14.8 Hz, C*H*$_2$Ph), 5.22 (d, 1H, $^{2}J_{H-H}$ = 14.8 Hz, C*H*$_2$Ph), 6.70 (s, 1H, C*H*=N, trz), 6.88 (d, 1H, $^{3}J_{P-H}$ = 7.41, C*H*OH), 6.92–6.96 (m, 1H, C*H*=, Ar), 7.04–7.10 (m, 4H, C*H*=, Ar), 7.15–7.24 (m, 6H, C*H*=, Ar), 7.30–7.32 (m, 6H, C*H*=, Ar), 7.41 (t, 1H, $^{3}J_{H-H}$ = 7.6 Hz, C*H*=, Ar), 7.90–7.93 (m, 1H, C*H*=, Ar). ^{13}C NMR (100 MHz, $CDCl_3$) δ: 17.2 (*C*H$_3$, OTBS), 24.8 (*t*-Bu, OTBS), 52.3 (*C*H_2Ph), 65.9 (d, $^{3}J_{C-P}$ = 29.2 Hz, *C*H–O), 120.8 (*C*H=N, trz), 125.7–133.7 (aromatic carbons), 134.8 (d, $^{1}J_{C-P}$ = 11.0 Hz, *C*=, Ar), 136.1 (d, $^{1}J_{C-P}$ = 11.0 Hz *C*=, Ar), 147.0 ($^{1}J_{C-P}$ = 22.0 Hz, *C*=, Ar), 150.3 (*C*=, Ar). MS HR-ESI [found 563.2513 $C_{34}H_{38}N_3OPSi$ $(M)^+$ requires 563.2517].

General Procedure for the Preparation of [Ir(cod)(L1)]BAr_F Catalyst Precursors

The corresponding ligand (0.037 mmol) was dissolved in CH_2Cl_2 (2 mL) and $[Ir(\mu\text{-}Cl)(cod)]_2$ (13.5 mg, 0.02 mmol) was added. The reaction mixture was stirred at 45 °C for 1 h. After 5 min at room temperature, $NaBAr_F$ (35 mg, 0.04 mmol) and degassed water (2 mL) were added and the reaction mixture was stirred vigorously for 30 min at room temperature. The phases were separated and the aqueous phase was extracted twice with CH_2Cl_2. The combined organic phases were dried with $MgSO_4$, evaporated in vacuo and purified by flash column chromatography (neutral SiO_2 *ca* 10 cm × 2 cm, 100% CH_2Cl_2).

[Ir(cod)(L1a)]BAr$_F$. Reaction carried out using **L1a** (22.4 mg, 0.037 mmol). Red-orange solid (60 mg, 89% yield). ^{31}P NMR (162 MHz, $CDCl_3$) δ: −5.9. ^{1}H NMR (400 MHz, $CDCl_3$) δ: 0.93–0.95 (m, 18H, C*H*$_3$, *i*-Pr), 1.06–1.11 (m, 3H, C*H*, *i*-Pr), 1.81 (m, 1H, C*H*$_2$, cod), 1.95–1.96 (m, 1H, C*H*$_2$, cod), 2.09–2.24 (m, 4H, C*H*$_2$, cod), 2.37–2.44 (m, 2H, C*H*$_2$, cod), 3.21 (m, 1H, C*H*, cod), 3.75 (m, 1H, C*H*, cod), 4.46 (m, 1H, C*H*, cod), 5.24 (d, 1H, $^{2}J_{H-H}$ = 13.4 Hz, C*H*$_2$Ph), 5.34 (d, 1H, $^{2}J_{H-H}$ = 13.4 Hz, C*H*$_2$Ph), 5.68 (m, 1H, C*H*, cod), 6.92 (d, 1H, $^{3}J_{H-H}$ = 7.7 Hz, C*H*=N, trz), 7.03 (t, 1H, $^{3}J_{H-H}$ = 8.5 Hz, C*H*=, Ar), 7.25–7.52 (m, 22H, C*H*O, C*H*=, Ar), 7.71 (s, 8H, C*H*=, Ar), 7.94–7.97 (m, 1H, C*H*=, Ar). ^{13}C NMR (100 MHz, $CDCl_3$) δ: 11.8 (*C*H, *i*-Pr), 17.7 (*C*H$_3$, *i*-Pr), 29.5 (*C*H_2, cod), 30.6 (*C*H_2, cod), 31.4 (*C*H_2, cod), 33.5 (*C*H_2, cod), 56.0 (*C*H_2Ph), 67.6 (*C*H, cod), 68.1 (*C*H, cod), 68.8 (d, $^{3}J_{C-P}$ = 15.1 Hz, *C*HO), 91.2 (d, $^{3}J_{C-P}$ = 12.3, *C*H, cod), 95.0 (d, $^{3}J_{C-P}$ = 12.3, *C*H, cod), 117.4–135.9 (aromatic carbons), 127.8 (*C*H=N, trz), 145.7 (d, $^{1}J_{C-P}$ = 13.0 Hz, *C*=, Ar), 154.5 (*C*=, Ar), 161.7 (q, $^{1}J_{C\text{-}B}$ = 50.0 Hz, *C*=, Ar). MS HR-ESI [found 906.2375 $C_{45}H_{56}IrN_3OPSi$ $(M)^+$ requires 906.2382].

Ir(cod)(L1b)]BAr$_F$. Reaction carried out using **L1b** (20.8 mg, 0.037 mmol). Red-orange solid (57.5 mg, 90% yield). ^{31}P NMR (162 MHz, $CDCl_3$) δ: 6.5. ^{1}H NMR (400 MHz, $CDCl_3$) δ: −0.01 (s, 3H, C*H*$_3$, OTBS), 0.11 (s, 3H, C*H*$_3$, OTBS), 0.90 (s, 9H, *t*-Bu, OTBS), 1.79–1.84 (m, 1H, C*H*$_2$, cod), 1.96–1.99 (m, 1H, C*H*$_2$, cod), 2.16–2.29 (m, 4H, C*H*$_2$, cod), 2.34–2.47 (m, 2H, C*H*$_2$, cod), 3.22–3.26 (m, 1H, C*H*, cod), 3.83–3.87 (m, 1H, C*H*, cod), 4.45–4.49 (m, 1H, C*H*, cod), 5.24 (s, 2H, C*H*$_2$Ph), 5.55–5.67 (m, 1H, C*H*, cod), 6.90 (d, 1H, $^{3}J_{H-H}$ = 7.7 Hz, C*H*=N, trz), 7.04 (t, 1H, $^{3}J_{H-H}$ = 9.6 Hz, C*H*=, Ar), 7.23–7.57 (m, 22H, C*H*O, C*H*=, Ar), 7.73 (s, 8H, C*H*=, Ar), 7.92–7.95 (m, 1H, C*H*=, Ar). ^{13}C NMR (100 MHz, $CDCl_3$) δ: −5.23 (*C*H$_3$, OTBS), −5.11 (*C*H$_3$, OTBS), 25.5 (*t*-Bu, OTBS), 29.2 (*C*H_2, cod), 29.7 (*C*H_2, cod), 31.1 (*C*H_2, cod), 34.0 (*C*H_2, cod), 55.9 (*C*H_2Ph), 67.3 (*C*H, cod), 68.2 (*C*H, cod), 69.1 (d, $^{3}J_{C-P}$ = 10.5 Hz, *C*HOH), 91.1 (d, $^{3}J_{C-P}$ = 11.0, *C*H, cod), 96.1 (d, $^{3}J_{C-P}$ = 11.0, *C*H, cod), 117.3–136.5 (aromatic carbons), 127.9 (*C*H=N, trz), 145.5 (d, $^{1}J_{C-P}$ = 14.3 Hz, *C*=, Ar), 154.3 (*C*=, Ar), 161.6 (q, $^{1}J_{C\text{-}B}$ = 50.0 Hz, *C*=, Ar). MS HR-ESI [found 864.3081 $C_{42}H_{50}IrN_3OPSi$ $(M)^+$ requires 864.3085].

General Procedure for the Asymmetric Hydrogenation

The alkene (0.125 mmol) and the corresponding catalyst precursor [Ir(cod)(**L**)]BAr_F (1 mol%) were dissolved in the corresponding solvent (1 mL) and placed in a high-pressure

autoclave. The autoclave was purged 4 times with hydrogen. Then, it was pressurized at the desired pressure. After 4 h, the autoclave was depressurized and the solvent evaporated off. The residue was dissolved in Et_2O (1.5 ml) and filtered through a short plug of silica. Conversions were determined by ^1H NMR and the enantiomeric excesses were determined by GC or HPLC (see Supporting Information for details).

Calculation Details

The calculations were carried out using B3LYP[16]-D3[17] functional as implemented in Gaussian 09.[18] For the geometry optimizations, the LANL2DZ[19] pseudopotential was used for iridium, and the 6-31G*[20] basis set was used for all other atoms. Implicit solvation using PCM[21] model with the parameters for dichloromethane was included in the geometry optimization. To obtain better accuracy, single-point calculations were carried out on the basis of the optimized geometries with the same basis set for iridium and the 6-311 + G**[22] basis set for the other atoms. The reported energies are Gibbs free energies in solution.

NCI-plot method was used to study the non-covalent interactions. The method is capable of mapping real-space regions where non-covalent interactions are important and is based exclusively on the electron density and its gradient. The information provided by NCI plots is essentially qualitative. Promolecular approximation using xyz files was used to perform these calculations.

Acknowledgements

Grant PID2019-104904GB–I00 funded by MCIN/AEI/10.13039/501100011033 and grant 2017SGR1472 funded by the Catalan Government are gratefully acknowledged. We also thank Dr. Maria Besora for her advice and suggestions on the DFT calculations.

References

[1] a) *Comprehensive Asymmetric Catalysis* (Eds.: E. N. Jacobsen, A. Pfaltz, H. Yamamoto), Springer-Verlag, Berlin, **1999**; b) *Catalytic Asymmetric Synthesis*, *3rd ed.* (Ed.: I. Ojima), John Wiley & Sons, Inc., Hoboken, **2010**; c) *Asymmetric Catalysis on Industrial Scale: Challenges, Approaches and Solutions*, *2nd ed.* (Eds.: H.-U. Blaser, H.-J. Federsel), Wiley-VCH, Weinheim, **2010**; d) C. A. Busacca, D. R. Fandrick, J. J. Song, C. H. Senanayake, *Adv. Synth. Catal.* **2011**, *353*, 1825–1864; e) D. J. Ager, A. H. M. de Vries, J. G. de Vries, *Chem. Soc. Rev.* **2012**, *41*, 3340–3380; f) *Metal-catalyzed Asymmetric Hydrogenation. Evolution and Prospect* in Advances in Catalysis (Eds.: M. Diéguez, A. Pizzano), Elsevier, Oxford, Vol. 68, **2021**.

[2] M. A. Stoffels, F. J. R. Klauck, T. Hamadi, F. Glorius, J. Leker, *Adv. Synth. Catal.* **2020**, *362*, 1258–1274.

[3] See for example: a) J.-P. Genêt, in *Modern Reduction Methods*, (Eds.: P. G. Andersson, I. J. Munslow), Wiley-VCH: Weinheim, **2008**; b) W. Tang, X. Zhang, *Chem. Rev.* **2003**, *103*, 3029–3069; c) Y. Chi, W. Tang, X. Zhang, In *Modern Rhodium-Catalyzed Organic Reactions*, (Ed.: P. A. Evans), Wiley-VCH: Weinheim, **2005**; d) M. Kitamura, R. Noyori, in *Ruthenium in Organic Synthesis*, (Ed.: S.-I. Murahashi), Wiley-VCH: Weinheim, **2004**; e) B. Weiner, W. Szymanski, D. B. Janssen, A. J. Minnaard, B. L. Feringa, *Chem. Soc. Rev.* **2010**, *39*, 1656–1691; f) J.-H. Xie, S.-F. Zhu, Q.-L. Zhou, *Chem. Rev.* **2011**, *111*, 1713–1760; g) P. Etayo, A. Vidal-Ferran, *Chem. Soc. Rev.* **2013**, *42*, 728–754; h) A. Pizzano, *Adv. Catal.* **2021**, *68*, 1–134; i) A. N. Kim, B. M. Stoltz, *ACS Catal.* **2020**, *10*, 13834–13851; j) A. Cabré, X. Verdaguer, A. Riera, *Chem. Rev.* **2022**, *122*, 269–339; k) Z. Zhang, N. A. Butt, W. Zhang, *Chem. Rev.* **2016**, *16*, 14769–14827.

[4] See for example: a) X. Cui, K. Burgess, *Chem. Rev.* **2005**, *105*, 3272–3296; b) S. J. Roseblade, A. Pfaltz, *Acc. Chem. Res.* **2007**, *40*, 1402–1411; c) D. H. Woodmansee, A. Pfaltz, *Chem. Commun.* **2011**, *47*, 7912–7916; d) Y. Zhu, K. Burgess, *Acc. Chem. Res.* **2012**, *45*, 1623–1636; e) J. J. Verendel, O. Pàmies, M. Diéguez, P. G. Andersson, *Chem. Rev.* **2014**, *114*, 2130–2169; f) C. Margarita, P. G. Andersson, *J. Am. Chem. Soc.* **2017**, *139*, 1346–1356; g) O. Pàmies, J. Zheng, J. Faiges, P. G. Andersson, *Adv. Catal.* **2021**, *68*, 135–203.

[5] See for instance: a) S.-Y. Shao, C. Wang, S.-W. Han, M.-H. Suna, S. Li, *Org. Biomol. Chem.* **2019**, *17*, 567–572; b) W. Amberg, U. E. W. Lange, M. Ochse, F. Pohlki, B. Behl, A. L. Relo, W. Hornberger, C. Hoft, M. Mezler, J. Sydor, Y. Wang, H. Zhao, J. T. Brewer, J. Dietrich, H. Li, I. Akritopoulou-Zanze, Y. Lao, S. M. Hannick, Y.-Y. Ku, A. Vasudevan, *J. Med. Chem.* **2018**, *61*, 7503–7524; c) Y. Donde, J. H. Nguyen, WO2015048553 A1, **2015**; d) F. Pohlki, U. Lange, M. Ochse, B. Behi, C. W. Hutchins, US2012040948 A1, **2012**; e) H. T. Sock, N. M. Teerhuis, G. H. Veeneman, US20100240748 A1, **2010**; f) P. T. Lansbury, C. J. Justman, WO2009036275 A1, **2009**; g) K. Yoshikawa, K. Suzuki, A. Umeyama, S. Arihara, *Chem. Pharm. Bull.* **2006**, *54*, 574–578; h) M. Numazawa, M. Ando, Y. Watari, T. Tominaga, Y. Hayata, A. Yoshimura, *J. Steroid Biochem. Mol. Biol.* **2005**, *96* 51–58; i) R. Kolanos, U. Siripurapu, M. Pullagurla, M. Riaz, V. Setola, B. L. Roth, M. Dukata, R. A. Glennona, *Bioorg. Med. Chem. Lett.* **2005**, *15*, 1987–1991.

[6] a) J. Xia, G. Yang, R. Zhuge, Y. Liu, W. Zhang, *Chem. Eur. J.* **2016**, *22*, 18354–18357; b) M. Biosca, M. Magre, M. Coll, O. Pàmies, M. Diéguez, *Adv. Synth. Catal.* **2017**, *359*, 2801–2814; c) M. Biosca, M. Magre, O. Pàmies, M. Diéguez, *ACS Catal.* **2018**, *8*, 10316–10320.

[7] See for instance: a) F. Tian, D. Yao, Y. Liu, F. Xie, W. Zhang, *Adv. Synth. Catal.* **2010**, *352*, 1841–1845; b) X. Liu, Z. Han, Z. Wang, K. Ding, *Angew. Chem.* **2014**, *126*, 2009–2013; *Angew. Chem. Int. Ed.* **2014**, *53*, 1978–1982; c) M. Biosca, O. Pàmies, M. Diéguez, *J. Org. Chem.* **2019**, *84*, 8259–8266; d) J. Margalef, M. Biosca, P. Cruz-Sánchez, X. Caldentey, C. Rodríguez-Escrich, O.

Pàmies, M. A. Pericàs, M. Diéguez, *Adv. Synth. Catal.* **2021**, *363*, 4561–4574.
[8] See for example: a) M. Diéguez, J. Mazuela, O. Pàmies, J. J. Verendel, P. G. Andersson, *J. Am. Chem. Soc.* **2008**, *130*, 7208–7209; b) J. Mazuela, J. J. Verendel, M. Coll, B. Schäffner, A. Börner, P. G. Andersson, O. Pàmies, M. Diéguez, *J. Am. Chem. Soc.* **2009**, *131*, 12344–12353; c) J. Mazuela, P.-O. Norrby, P. G. Andersson, O. Pàmies, M. Diéguez, *J. Am. Chem. Soc.* **2011**, *133*, 13634–13645; d) M. Biosca, E. Salomó, P. de la Cruz-Sanchez, A. Riera, X. Verdaguer, O. Pàmies, M. Diéguez, *Org. Lett.* **2019**, *21*, 807–811.
[9] W. J. Drury III, N. Zimmermann, M. Keenan, M. Hayashi, S. Kaiser, R. Goddard, A. Pfaltz, *Angew. Chem.* **2004**, *116*, 72–76; *Angew. Chem. Int. Ed.* **2004**, *43*, 70–74.
[10] In addition, the introduction of a triazole instead of the commonly used oxazoline group made the synthetic route more straightforward. Thus, for instance, the modification of the procedure in similar phosphine-oxazoline with a methylene linker developed by Hou, Wu and coworkers would require 2–3 more additional steps making the synthesis less appealing. W.-Q. Wu, Q. Peng, D.-X. Dong, X.-L. Hou, Y.-D. Wu, *J. Am. Chem. Soc.* **2008**, *130*, 9717–9725.
[11] C. Hempel, C. Maichle-Mössmer, M. A. Pericàs, B. J. Nachtsheim, *Adv. Synth. Catal.* **2017**, *359*, 2931–2941.
[12] a) P. Brandt, C. Hedberg, P. G. Andersson, *Chem. Eur. J.* **2003**, *9*, 339–347; b) Y. Fan, X. Cui, K. Burgess, M. B. Hall, *J. Am. Chem. Soc.* **2004**, *126*, 16688–16689; c) X. Cui, Y. Fan, M. B. Hall, K. Burgess, *Chem. Eur. J.* **2005**, *11*, 6859–6868; d) T. L. Church, T. Rasmussen, P. G. Andersson, *Organometallics* **2010**, *29*, 6769–6781; e) K. H. Hopmann, A. Bayer, *Organometallics* **2011**, *30*, 2483–2497; f) S. Gruber, A. Pfaltz, *Angew. Chem.* **2014**, *126*, 1927–1931; *Angew. Chem. Int. Ed.* **2014**, *53*, 1896–1900.
[13] S. Aguado-Ullate, M. Urbano-Cuadrado, I. Villalba, E. Pires, J. I. García, C. Bo, J. J. Carbó, *Chem. Eur. J.* **2012**, *18*, 14026–14036.
[14] See also for example: a) K. Källström, C. Hedberg, P. Brandt, A. Bayer, P. G. Andersson, *J. Am. Chem. Soc.* **2004**, *126*, 14308–14309; b) J. Faiges, C. Borràs, I. M. Pastor, O. Pàmies, M. Besora, M. Diéguez, *Organometallics* **2021**, *40*, 3424–3435.
[15] For the TS_E the two CH–N interactions are located between the N of the triazole and the phenyl substituent of the substrate and the same N with one of the methylenic hydrogens of the tetrahydronaphthalene moiety. The T-shaped π–π interaction is found between the substrate phenyl ring and the benzyl substituent of the triazole.
[16] a) A. D. Becke, *J. Chem. Phys.* **1993**, *98*, 5648–5652; b) P. J. Stephens, F. J. Devlin, C. F. Chabalowski, M. J. Frisch, *J. Phys. Chem.* **1994**, *98*, 11623–11627.
[17] S. Grimme, J. Antony, S. Ehrlich, H. Krieg, *J. Chem. Phys.* **2010**, *132*, 154104.
[18] M. J. Frisch, G. W. Trucks, H. B. Schlegel, G. E. Scuseria, M. A. Robb, J. R. Cheeseman, G. Scalmani, V. Barone, G. A. Petersson, H. Nakatsuji, X. Li, M. Caricato, A. V. Marenich, J. Bloino, B. G. Janesko, R. Gomperts, B. Mennucci, H. P. Hratchian, J. V. Ortiz, A. F. Izmaylov, J. L. Sonnenberg, D. Williams-Young, F. Ding, F. Lipparini, F. Egidi, J. Goings, B. Peng, A. Petrone, T. Henderson, D. Ranasinghe, V. G. Zakrzewski, J. Gao, N. Rega, G. Zheng, W. Liang, M. Hada, M. Ehara, K. Toyota, R. Fukuda, J. Hasegawa, M. Ishida, T. Nakajima, Y. Honda, O. Kitao, H. Nakai, T. Vreven, K. Throssell, J. A. Montgomery, J. E. Peralta, F. Ogliaro, M. J. Bearpark, J. J. Heyd, E. N. Brothers, K. N. Kudin, V. N. Staroverov, T. A. Keith, R. Kobayashi, J. Normand, K. Raghavachari, A. P. Rendell, J. C. Burant, S. S. Iyengar, J. Tomasi, M. Cossi, J. M. Millam, M. Klene, C. Adamo, R. Cammi, J. W. Ochterski, R. L. Martin, K. Morokuma, O. Farkas, J. B. Foresman, D. J. Fox, Gaussian 16, Revision A.03. Gaussian, Inc.: Wallingford CT, **2016**.
[19] a) P. J. Hay, W. R. Wadt, *J. Chem. Phys.* **1985**, *82*, 270–283; b) P. J. Hay, W. R. Wadt, *J. Chem. Phys.* **1985**, *82*, 299–310.
[20] a) W. J. Hehre, R. Ditchfield, J. A. Pople, *J. Chem. Phys.* **1972**, *56*, 2257–2261; b) P. C. Hariharan, J. A. Pople, *Theor. Chim. Acta* **1973**, *28*, 213–222; c) M. M. Francl, W. J. Pietro, W. J. Hehre, J. S. Binkley, M. S. Gordon, D. J. Defrees, J. A. Pople, *J. Chem. Phys.* **1982**, *77*, 3654–3665.
[21] J. Tomasi, B. Mennucci, R. Cammi, *Chem. Rev.* **2005**, *105*, 2999–3094.
[22] a) R. Krishnan, J. S. Binkley, R. Seeger, J. A. Pople, *J. Chem. Phys.* **1980**, *72*, 650–654; b) A. D. McLean, G. S. Chandler, *J. Chem. Phys.* **1980**, *72*, 5639–5648.